Covalently Linked Oxomolybdenum(V) and Iron(III) Porphyrin Centers: Synthetic Models for the Molybdenum-Iron Interaction in Sulfite Oxidase

Partha Basu, Arnold M. Raitsimring, Michael J. LaBarre, Ish K. Dhawan, Jeff L. Weibrecht,† and John H. Enemark*

Contribution from the Department of Chemistry, University of Arizona, Tucson, Arizona 85721

Received January 18, 1994®

Abstract: The modified tetraarylporphyrins 5-(3,4-dihydroxyphenyl)-10,15,20-tri-*p*-tolylporphyrin (3,4-OH-TTP, **3**) and 5-(2,3-dihydroxyphenyl)-10,15,20-tri-*p*-tolylporphyrin (2,3-OH-TTP, **4**) that possess a single pendant catechol group at one of the meso positions have been synthesized and used to investigate the coupling between oxo-Mo(V) and Fe(III) centers as preliminary models for the inter-prosthetic group interaction in sulfite oxidase. Reaction of these novel ligands with $LMoO^{2+}$ (L = hydrotris(3,5-dimethyl-1-pyrazolyl)borate) followed by insertion of Fe(III) into the porphyrin generates the bimetallic complexes FeCl(3,4-Mo-TTP) (**11**) and FeCl(2,3-Mo-TTP) (**12**) with controlled Mo···Fe distances of 9.4 and 7.3 Å, respectively, as determined from computer modeling. Addition of excess *N*-methylimidazole (*N*-MeIm) produces the six-coordinate complexes Fe(*N*-MeIm)$_2$(3,4-Mo-TTP)Cl (**13**) and Fe(*N*-MeIm)$_2$(2,3-Mo-TTP)Cl (**14**) with low-spin Fe(III) centers and two axial imidazole ligands. The formation constants for these bimetallic bis(*N*-methylimidazole) complexes are larger than those for related six-coordinated monometallic Fe(III) complexes of asymmetric porphyrin ligands. The interaction between the two $S = {}^1/_2$ metal centers of Fe(*N*-MeIm)$_2$(3,4-Mo-TTP)Cl and Fe(*N*-MeIm)$_2$(2,3-Mo-TTP)Cl has been probed by cyclic voltammetry and EPR spectroscopy. Simulation of the EPR spectra of these bimetallic Mo···Fe complexes shows that weak anisotropic dipolar coupling dominates the interaction between the two metals in Fe(*N*-MeIm)$_2$(3,4-Mo-TTP)Cl (Mo···Fe ~ 9.4 Å), whereas weak exchange interactions ((3–70) × 10^{-3} cm^{-1}, 100–2000 MHz) predominate for Fe(*N*-MeIm)$_2$(2,3-Mo-TTP)Cl (Mo···Fe ~ 7.9 Å). The EPR simulations for both Fe(*N*-MeIm)$_2$(3,4-Mo-TTP)Cl and Fe(*N*-MeIm)$_2$(2,3-Mo-TTP)Cl require a distribution of coupling interaction energies, consistent with the presence of several rotamers of the *N*-methylimidazole ligand in solution that produce different orientations of the in-plane magnetic axes of the porphyrin. Cyclic voltammetry shows that two metal centers of Fe(*N*-MeIm)$_2$(3,4-Mo-TTP)Cl and Fe(*N*-MeIm)$_2$(2,3-Mo-TTP)Cl behave essentially as independent one-electron couples, but the potential of the Mo(V/IV) couple is sensitive to the electronic state and charge on the metalloporphyrin core.

Introduction

Sulfite oxidase is a pterin-containing molybdenum enzyme[1] that resides in the mitochondrial intermembrane space and catalyzes the physiologically vital oxidation of sulfite to sulfate.[2,3] Each identical subunit of the dimeric enzyme has a molecular weight of about 55 000 and possesses one pterin-containing molybdenum cofactor and one cytochrome b_5-type heme.[4-6] The two-electron oxidation of sulfite to sulfate most likely involves an oxygen atom-transfer reaction[1] from a dioxo-Mo(VI) center with concomitant formation of a monooxo-Mo(IV) center. Such chemistry is well known for model systems[1,7-9] and has also been shown to be a step in the catalytic cycle of xanthine oxidase,[10] another pterin-containing molybdenum enzyme.

Regeneration of the catalytically active molybdenum center of pterin-containing enzymes probably involves coupled electron-proton-transfer reactions.[1,7a,11] For sulfite oxidase, two *intramolecular* one-electron transfers from the Mo center to the *b*-type heme center are proposed to occur during the catalytic cycle[12] (Figure 1). Our recent laser flash photolysis studies[13] have shown that intramolecular electron transfer between the Fe(II)/Mo(VI) oxidation states of sulfite oxidase is strongly inhibited by anions in the media.[13a,b] There is presently no structural basis for interpreting these results because the crystal structure of sulfite oxidase has not been determined, and the distance between the molybdenum and iron centers is unknown.

The goal of this research is to synthesize a series of well-characterized model compounds that can be used to quantitatively

* Author to whom correspondence should be addressed.
† High School Student Intern.
® Abstract published in *Advance ACS Abstracts*, July 1, 1994.

(1) Enemark, J. H.; Young, C. G. *Adv. Inorg. Chem.* **1993**, *40*, 1–88.
(2) Rajagopalan, K. V. In *Advances in Enzymology and Related Areas of Molecular Biology*; Meister, A., Ed.; John Wiley & Sons, Inc.: New York City, NY, 1991; Vol. 64, pp 215–290.
(3) (a) Burgmayer, S. J. N.; Stiefel, E. I. *J. Chem. Educ.* **1985**, *62*, 943–953. (b) Pilato, R. S.; Stiefel, E. I. In *Inorganic Catalysis*; Reedijk, J., Ed.; Marcel Dekker, Inc.: New York, 1993; pp 131–188.
(4) Neame, P. J.; Barber, M. J. *J. Biol. Chem.* **1989**, *264*, 20894–20901.
(5) Cohen, H. J.; Fridovich, I. *J. Biol. Chem.* **1971**, *246*, 359–366; 367–373.
(6) (a) Johnson, J. L.; Rajagopalan, K. V. *J. Clin. Invest.* **1976**, *58*, 543–550. (b) Gardlik, S.; Rajagopalan, K. V. *J. Biol. Chem.* **1990**, *265*, 13047–13054. (c) Gardlik, S.; Rajagopalan, K. V. *J. Biol. Chem.* **1991**, *266*, 4889–4895. (d) Rajagopalan, K. V. *Biochem. Elem.* **1984**, *3*, 149.
(7) (a) Xiao, Z.; Young, C. G.; Enemark, J. H.; Wedd, A. G. *J. Am. Chem. Soc.* **1992**, *114*, 9194–9195. (b) Young, C. G.; Wedd, A. G. In *Molybdenum Enzymes, Cofactors and Model Systems*; Stiefel, E. I., Coucouvanis, D., Newton, W. E., Eds.; ACS Symposium Series 535; American Chemical Society: Washington, DC, 1993; pp 70–82.
(8) (a) Roberts, S. A.; Young, C. G.; Kipke, C. A.; Cleland, W. E., Jr.; Yamanouchi, K.; Carducci, M. D.; Enemark, J. H. *Inorg. Chem.* **1990**, *29*, 3650–3656. (b) Roberts, S. A.; Young, C. G.; Cleland, W. E., Jr.; Ortega, R. B.; Enemark, J. H. *Inorg. Chem.* **1988**, *27*, 3044–3051. (c) LaBarre, M. J.; Enemark, J. H. *J. Inorg. Biochem.* **1991**, *43*, 582.
(9) (a) Gheller, S. F.; Schultz, B. E.; Scott, M. J.; Holm, R. H. *J. Am. Chem. Soc.* **1992**, *114*, 6934–6935. (b) Holm, R. H. *Coord. Chem. Rev.* **1990**, *100*, 183–221. (c) Holm, R. H.; Berg, J. M. *Acc. Chem. Res.* **1986**, *19*, 363–370. (d) Holm, R. H. *Chem. Rev.* **1987**, *87*, 1401–1449.
(10) Hille, R.; Sprecher, H. *J. Biol. Chem.* **1987**, *262*, 10914–10917.
(11) Stiefel, E. I. *Proc. Natl. Acad. Sci. U.S.A.* **1973**, *70*, 988.
(12) (a) Speck, S. H.; Koppenol, W. H.; Dethmers, J. K.; Osheroff, N.; Margoliasch, E.; Rajagopalan, K. V. *J. Biol. Chem.* **1981**, *256*, 7394–7400. (b) Rajagopalan, K. V. In *Molybdenum and Molybdenum Containing Enzymes*; Coughlan, M., Ed.; Pergamon Press: New York, 1980; pp 243–272.
(13) (a) Sullivan, E. P., Jr.; Hazzard, J. T.; Tollin, G.; Enemark, J. H. *Biochemistry* **1993**, *32*, 12465–12470. (b) Sullivan, E. P., Jr.; Hazzard, J. T.; Tollin, G.; Enemark, J. H. *J. Am. Chem. Soc.* **1992**, *114*, 9662–9663. (c) Kipke, C. A.; Cusanovich, M. A.; Tollin, G.; Sunde, R. A.; Enemark, J. H. *Biochemistry* **1988**, *27*, 2918–2926.

0002-7863/94/1516-7166$04.50/0

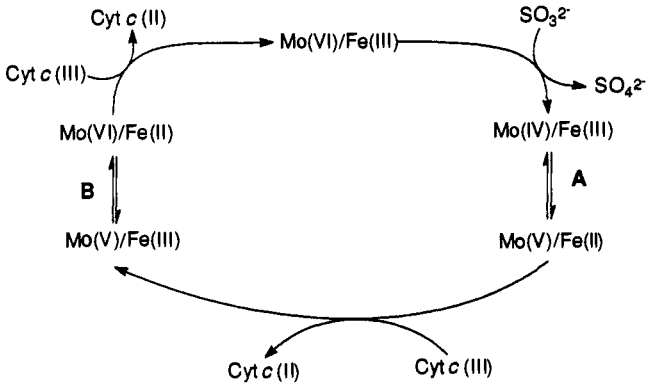

Figure 1. Proposed catalytic cycle for sulfite oxidase, adapted from ref 12b. A is the intramolecular electron-transfer reaction for the two-electron reduced state of the enzyme. B is the intramolecular electron-transfer reaction for the one-electron reduced state.

probe the interactions between an oxomolybdenum center and an iron porphyrin center as a function of the molybdenum–iron distance. Our initial approach has been to synthesize bimetallic compounds of the type shown in Figure 2 that possess both an oxo-Mo(V) center and a Fe(III) porphyrin center that are covalently linked through a rigid intervening organic backbone that can be systematically varied in order to change the Mo···Fe internuclear distance. In the enzyme itself, the two prosthetic groups are unlikely to be covalently linked, but these synthetic models allow us to begin to quantitate the factors that are important in inter-prosthetic group interactions in sulfite oxidase. The iron atom is coordinated by a modified tetratolylporphyrin ring system in which one of the tolyl groups has been replaced by a catechol ring. An oxo-Mo(V) center stabilized by the tridentate and facially coordinating hydrotris(3,5-dimethyl-1-pyrazolyl)borate ligand (L)[14–16] is attached to the pendant catecholate moiety. To a first approximation, the metal–metal distance will not be significantly affected by ruffling of the porphyrin ring[17] or rotation about the C–C bond linking the methine carbon of the porphyrin ring to the catecholate group coordinated to the oxo-Mo(V) center. Herein we report the synthesis and properties of the modified porphyrins and several complexes. The weak coupling between Mo(V) and Fe(III) has been probed by EPR spectroscopy and electrochemistry.

Experimental Section

Materials. Reactions were carried out in air unless specified otherwise. All anaerobic reactions were performed using standard inert atmosphere techniques with argon presaturated with the appropriate solvent. Subsequent workups of all reactions were carried out in air. Solvents used were purified by distillation and thoroughly degassed before use: tetrahydrofuran (THF) from potassium, dichloromethane (DCM) and methanol (MeOH) from calcium hydride, and toluene from sodium. Dimethylformamide (DMF) was purchased as Aldrich anhydrous grade and used as received. Chromatography was conducted using glass columns packed with Sigma S-2509 silica gel. Tetraethylammonium perchlorate (TEAP) was prepared according to the literature method.[18] Pyrrole, tolualdehyde, propionic acid, 2,3-dihydroxybenzaldehyde, 3,4-dihydroxybenzaldehyde, 2,3-dimethoxybenzaldehyde, 3,4-dimethoxybenzaldehyde, zinc chloride, iron(II) chloride tetrahydrate, dichloromethane-d_2 (CD_2Cl_2), and deuteriochloroform ($CDCl_3$) were purchased from Aldrich Chemical Co. and used as received. Potassium hydrotris(3,5-dimethyl-1-pyrazolyl)borate (KL),[14] catecholato(hydrotris(3,5-dimethyl-1-pyrazolyl)borato)oxomolybdenum(V) [LMo^VO(catechol)], and ethylene glycolato(hydrotris(3,5-dimethyl-1-pyrazolyl)borato)oxomolybdenum(V) [LMo^VO(eth-gly)] were prepared according to published methods.[16] 5,10,15,20-Tetra-*p*-tolylporphyrin (TTP)[19] and its zinc and chloroiron insertion products were prepared according to modifications of the published procedures.[19,20] The purity of isolated compounds and the progress of all reactions were monitored by thin-layer chromatography on silica gel plates and/or by observing the change in the electronic spectrum. Microanalyses were performed by Atlantic Microlab Inc., Atlanta, GA.

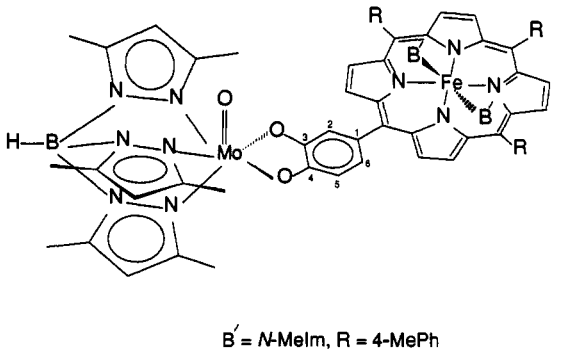

Figure 2. Model bimetallic complex possessing oxo-Mo(V) and Fe(III) porphyrin centers, cf. **13**. B′ = *N*-MeIm; R = 4-MePh.

Physical Measurements. Infrared spectra were recorded on a Perkin-Elmer 983 spectrophotometer with samples as KBr pellets unless otherwise noted. Cyclic voltammetry was performed using a BAS CV-50W system with a three-electrode configuration. The reference electrode was a silver/silver chloride electrode (Ag/AgCl), a BAS Model MF-2012 graphite electrode was used as the working electrode, and a platinum wire served as the counter electrode. The sample concentrations were ~1 mM, the concentration of *N*-methylimidazole was ~0.1 M, and the supporting electrolyte was tetraethylammonium perchlorate at 100 mM. All half-wave potentials were internally referenced against the ferrocenium/ferrocene couple and expressed with respect to the saturated calomel electrode, SCE. ^{1}H NMR spectra were recorded on Bruker AM-250, AM-500, or UNITY-300 spectrometers. For diamagnetic compounds, a 6-kHz spectral width, a 32*K* data block, and a 30° pulse width were used; for paramagnetic compounds, a 30–100 kHz spectra width, a 32*K* data block, and a 45° or 90° pulse width were used. All resonances are referenced to internal residual proton resonances of CD_2Cl_2 (δ 5.32) or $CDCl_3$ (δ 7.24). Electronic spectra were recorded on a modified Cary 14 spectrophotometer equipped with an OLIS interface and software. The cuvette compartment was attached to a circulating propylene glycol constant temperature bath which maintained the cuvette temperature at 25.0 ± 0.5 °C. Electron paramagnetic resonance (EPR) spectra were obtained with a Bruker ESP 300E spectrometer. Samples were prepared as 0.5–2 mM solutions in a toluene:dichloromethane (1:1) glass. Liquid nitrogen temperature was maintained using a quartz immersion Dewar. Mass spectra were obtained at the University of Arizona Department of Pharmacy Mass Spectral Facility. The spectra were recorded on a modified Magnetic Sector AMD Intectra instrument utilizing FAB and liquid SIMS techniques on nitrobenzyl alcohol solutions, and molecular masses are reliable to ±0.5 amu.

Preparation of Compounds. 5-(3,4-Dimethoxyphenyl)-10,15,20-tri-*p*-tolylporphyrin (3,4-OMe-TTP, 1). 3,4-Dimethoxybenzaldehyde (8.3 g, 50 mmol) and *p*-tolualdehyde (18 g, 150 mmol) were dissolved in propionic acid (500 mL) and brought to reflux. Freshly distilled pyrrole (13.4 g, 200 mmol) was added, and the reflux was continued for 45 min. The reaction mixture was cooled to 11 °C, filtered, and washed with cold ethanol. The purple solid was purified by chromatography on a silica gel column with dichloromethane–hexane (75:25) as the eluant. TTP moved rapidly with the solvent front followed by the purple band of **1**. The product was collected and evaporated under vacuum. Recrystallization of **1** from dichloromethane–heptane solution gave shiny purple crystals. Yield: 0.70 g (2%).

(14) Trofimenko, S. *J. Am. Chem. Soc.* **1967**, *89*, 6288–6294.
(15) Rowley, N. M.; Kurek, S. S.; George, M. W.; Hubig, S. M.; Beer, P. D.; Jones, C. J.; Kelly, J. M.; McCleverty, J. A. *J. Chem. Soc., Chem. Commun.* **1992**, 497–499.
(16) Cleland, W. E., Jr.; Barnhart, K. M.; Yamanouchi, K.; Collision, D.; Mabbs, F. E.; Ortega, R. B.; Enemark, J. H. *Inorg. Chem.* **1987**, *26*, 1017–1025.
(17) Safo, M. K.; Gupta, G. P.; Watson, C. T.; Simonis, U.; Walker, F. A.; Scheidt, W. R. *J. Am. Chem. Soc.* **1992**, *114*, 7066–7075.
(18) Sawyer, D. T.; Roberts, J. L., Jr. *Experimental Electrochemistry for Chemists*; Wiley: New York, 1974; p 212.
(19) (a) Adler, A. D.; Longo, F. R.; Finarelli, J. D.; Goldmacher, J.; Assour, J.; Korsakoff, L. *J. Org. Chem.* **1957**, *32*, 476. (b) Adler, A. D.; Longo, F. R.; Kampas, F.; Kim, J. *J. Inorg. Nucl. Chem.* **1970**, *32*, 2443–2445.
(20) Walker, F. A.; Simonis, U. In *Encyclopedia of Inorganic Chemistry*; King, R. B., Ed.; Wiley & Sons, Ltd.: London, in press.

^{1}H NMR ($CDCl_3$): δ 2.69 (s, 9H); 3.97 (s, 3H); 4 (s, 3H); 7.23 (d, J = 8 Hz, 1H); 7.54 (d, J = 8 Hz, 6H); 7.74 (d, J = 8 Hz, 1H); 7.76 (s, 1H); 8.1 (d, J = 8 Hz, 6H); 8.85 (m, 8H). Mass spectrum: calculated molecular ion, 716.32 amu; found, 717.00 amu. Anal. Calcd for $C_{49}H_{40}N_4O_2$: C, 82.07; H, 5.62; N, 7.85. Found: C, 80.90; H, 5.75; N, 7.72.

5-(2,3-Dimethoxyphenyl)-10,15,20-tri-*p*-tolylporphyrin (2,3-OMe-TTP,[21] 2) was prepared from 2,3-dimethoxybenzaldehyde according to the procedure used for **1**, and the crude product was purified by adsorption chromatography on silica gel with dichloromethane–hexane (1:1) as the eluant. Recrystallization was from dichloromethane–heptane. Yield: 1–1.5%.

^{1}H NMR ($CDCl_3$): δ 2.70 (s, 9H); 3.18 (s, 3H); 4.13 (s, 3H); 7.38 (m, 2H); 7.55 (d, J = 8 Hz, 6H); 7.65 (m, 1H); 8.1 (m, 6H); 8.3 (m, 8H). Mass spectrum: calculated molecular ion, 716.32 amu; found, 716.60.

5-(3,4-Dihydroxyphenyl)-10,15,20-tri-*p*-tolylporphyrin (3,4-OH-TTP, 3). A solution of 0.2 g (2.8×10^{-4} mol) of **1** dissolved in a minimum volume of freshly distilled dichloromethane was added dropwise to a BBr_3 solution (2 mL of BBr_3 in 5 mL of dichloromethane) at –80 °C. The solution was stirred for 1 h, slowly brought to room temperature, and then stirred for an additional 24 h. Water was added slowly to the green solution to hydrolyze any excess BBr_3 present, and the solution was neutralized with triethylamine to precipitate a purple solid. The solid mass was filtered, washed with water, dried, and recrystallized from dichloromethane–heptane solution. Yield: 0.17 g (90%).

^{1}H NMR (CD_2Cl_2): δ 2.70 (s, 9H); 7.12 (d, J = 8Hz, 1H); 7.49 (s, 1H); 7.57 (d, J = 8 Hz, 7H); 8.09 (d, J = 8 Hz, 6H); 8.87 (s, 8H). Mass spectrum: calculated molecular ion, 688.28 amu; found, 688.20 amu. Anal. Calcd for $C_{47}H_{36}N_4O_2$: C, 81.92; H, 5.27; N, 8.17. Found: C, 81.49; H, 5.56; N, 7.92.

5-(2,3-Dihydroxyphenyl)-10,15,20-tri-*p*-tolylporphyrin (2,3-OH-TTP,[21] 4) was prepared from **2** according to the method described above for **3**. Yield: 0.65 g (88%).

^{1}H NMR (CD_2Cl_2): δ 2.71 (s, 9H); 7.23 (t, J = 8 Hz, 1H); 7.33 (d, J = 8 Hz, 1H); 7.59 (d, J = 8 Hz, 7H); 8.10 (*d*, J = 8 Hz, 6H); 8.89 (m, 8H). Mass spectrum: calculated molecular ion, 688.28 amu; found, 689.45 amu. Anal. Calcd for $C_{47}H_{36}N_4O_2$: C, 81.92; H, 5.27; N, 8.17. Found: C, 80.86; H, 5.62; N, 7.87.

Compounds **3** and **4** can also be synthesized in similar overall yield from the direct reaction of the appropriate dihydroxybenzaldehyde and pyrrole.[22]

5-(3,4-Dimethoxyphenyl)-10,15,20-tri-*p*-tolylporphyrinatoiron(III) Chloride (FeCl(3,4-OMe-TTP), 5). Iron insertion was done in DMF according to Adler's method[19b] but using aqueous HCl in the workup. After the iron insertion was complete as evidenced by the electronic spectrum, the solvent was evaporated in vacuo at elevated temperature. The crude product was dissolved in dichloromethane and washed with water in order to remove inorganic salts and any remaining DMF. The organic layer was subjected to chromatography on a silica gel column. The μ-oxo species eluted as a brownish green band with dichloromethane. This fraction was then shaken vigorously with aqueous HCl to convert the μ-oxo species into the chlorinated species. Evaporation of the organic layer followed by recrystallization from dichloromethane–heptane gave pure solid product. Yield: 65%.

Mass spectrum: calculated molecular ion, 806.20 amu; found, 770.20 amu (M – Cl = 770.23). Anal. Calcd for $C_{49}H_{38}N_4O_2FeCl$: C, 72.98; H, 4.75; N, 6.98; Cl, 4.40. Found: C, 72.73; H, 5.02; N, 6.80; Cl, 4.26.

5-(2,3-Dimethoxyphenyl)-10,15,20-tri-*p*-tolylporphyrinatoiron(III) Chloride (FeCl(2,3-OMe-TTP), 6). This compound was prepared similarly to **5**. Yield: 67%.

Mass spectrum: calculated molecular ion, 806.20 amu; found, 770.20 amu (M – Cl = 770.23).

5-(3,4-Catecholato(hydrotris(3,5-dimethyl-1-pyrazolyl)borato)oxomolybdenum(V))-10,15,20-tri-*p*-tolylporphyrin (3,4-Mo-TTP, 7). **3** (0.5 g, 0.7 mmol) and LMo^VO(eth-gly) (0.7 g, 1.5 mmol) were placed in an evacuated Schlenk flask (250 mL). Degassed toluene (100 mL) was added, and the mixture was brought to a mild reflux with stirring. Heating was continued until the reaction was complete as evidenced by thin-layer chromatography. Toluene was removed under vacuum at elevated temperature. Dichloromethane–toluene (1:1) (25 mL) was added to yield a purple/brown solution. The solution was purified by chromatography on a silica gel column (3 × 30 cm) with dichloromethane–toluene (1:1) as eluant. The solvent was removed in vacuo. Recrystallization from dichloromethane–heptane gave dark purple microcrystals. Yield: 0.65 g (82%).

IR (KBr): ν(B—H) 2545 w; ν(Mo═O) 941 s. Mass spectrum: calculated molecular ion, 1097.37 amu; found, 1098.41 amu. Anal. Calcd for $C_{62}H_{56}N_{10}O_3MoB$: C, 67.95; H, 5.15; N, 12.78. Found: C, 67.88; H, 5.64; N, 12.24.

5-(2,3-Catecholato(hydrotris(3,5-dimethyl-1-pyrazolyl)borato)oxomolybdenum(V))-10,15,20-tri-*p*-tolylporphyrin (2,3-Mo-TTP, 8) was synthesized according to the procedure for **7** but utilizing **4** as the substituted porphyrin. Yield: 0.70 g (88%).

Anal. Calcd for $C_{62}H_{56}N_{10}O_3MoB$: C, 67.95; H, 5.15; N, 12.78. Found: C, 68.10; H, 5.33; N, 12.62. IR (KBr): ν(B—M) 2547 w; ν(Mo═O) 939 s. Mass spectrum: calculated molecular ion, 1097.37 amu; found, 1096.52 amu.

5-(3,4-Catecholato(hydrotris(3,5-dimethyl-1-pyrazolyl)borato)oxomolybdenum(V))-10,15,20-tri-*p*-tolylporphinatozinc(II) (Zn(3,4-Mo-TTP), 9). **7** (0.175 g, 0.16 mmol) was dissolved in DMF (100 mL) and brought to reflux. $ZnCl_2$ (0.30 g, 2.2 mmol) was added to the solution with vigorous stirring. Reflux was maintained until zinc insertion was complete as evidenced by the loss of the bands from **7** in the electronic spectrum. DMF was removed under vacuum. Dichloromethane (50 mL) was added to yield a pink/purple solution. This solution was washed with 3 × 200-mL portions of water to remove inorganic zinc salts and the remaining DMF. The dichloromethane solution was purified by chromatography on silica gel with dichloromethane–methanol (20:1) as eluant. The solvent was removed in vacuo. Recrystallization from toluene–heptane gave purple microcrystals. Yield: 0.12 g (65%).

IR (KBr): ν(B—H) 2545 w; ν(Mo═O) 940 s. Mass spectrum: calculated molecular ion, 1159.29 amu; found, 1159.43 amu. Anal. Calcd for $C_{62}H_{54}N_{10}O_3MoBZn$: C, 64.20; H, 4.69; N, 12.13. Found: C, 65.73; H, 5.18; N, 11.17.

5-(2,3-Catecholato(hydrotris(3,5-dimethyl-1-pyrazolyl)borato)oxomolybdenum(V))-10,15,20-tri-*p*-tolylporphinatozinc(II) (Zn(2,3-Mo-TTP), 10). Compound **10** was synthesized from **8** according to the procedure for **9**. Yield: 0.10 g (60%).

IR (KBr): ν(B—H) 2542; ν(Mo═O) 940. Mass spectrum: calculated molecular ion, 1159.27 amu; found, 1159.43 amu. Anal. Calcd for $C_{62}H_{54}N_{10}O_3MoBZn$: C, 64.20; H, 4.69; N, 12.13. Found: C, 65.28; H, 5.03; N, 11.28.

5-(3,4-Catecholato(hydrotris(3,5-dimethyl-1-pyrazolyl)borato)oxomolybdenum(V))-10,15,20-tri-*p*-tolylporphinatoiron(III) Chloride (FeCl(3,4-Mo-TTP), 11). **7** (0.2 g, 1.82×10^{-4} mol) was dissolved in 20 mL of dichloromethane, and $FeCl_2 \cdot 4H_2O$ (0.2 g, 1.08×10^{-3} mol) was dissolved in 15 mL of a methanol–dichloromethane mixture. After addition of the iron solution to the porphyrin solution, the mixture was refluxed until iron insertion was complete as evidenced by the electronic spectra. The solution was evaporated to dryness under vacuum and dissolved in dichloromethane (50 mL) to yield a brown solution. After the solution was washed with 3 × 100-mL portions of water, the organic phase was purified by chromatography on a silica gel column with dichloromethane–methanol (10:1) as eluant. The greenish brown fraction was evaporated, redissolved in dichloromethane (25 mL), and reacted with 2 × 200-mL portions of aqueous NaCl (1 M) with vigorous stirring. The remaining dichloromethane solution was washed with water (100 mL), and the solvent was removed in vacuo. Recrystallization from dichloromethane–heptane gave dark purple/black microcrystals. Yield: 0.14 g (65%).

IR (KBr): ν(B—H) 2545 w; ν(Mo═O) 940 s. Mass spectrum: calculated molecular ion, 1186.26 amu; found, 1150.63 amu (M – Cl = 1151.29 amu). Anal. Calcd for $C_{62}H_{54}N_{10}O_3MoBFeCl$: C, 62.79; H, 4.59; N, 11.86; Cl, 2.99. Found: C, 63.97; H, 5.40; N, 11.00; Cl, 2.82.

5-(2,3-Catecholato(hydrotris(3,5-dimethyl-1-pyrazolyl)borato)oxomolybdenum(V))-10,15,20-tri-*p*-tolylporphinatoiron(III) Chloride (FeCl(2,3-Mo-TTP), 12). This compound was synthesized according to the procedure for **11**, utilizing **8** as the molybdenum-containing porphyrin. Recrystallization from dichloromethane–heptane gave a purple powder. Yield: 80 mg (75%).

Anal. Calcd for $C_{62}H_{54}N_{10}O_3MoBFeCl$: C, 62.79; H, 4.59; N, 11.86; Cl, 2.99. Found: C, 62.69; H, 4.78; N, 11.88; Cl, 3.06. IR (KBr): ν(B—H) 2550 w; ν(Mo═O) 943 s. Mass spectrum: calculated molecular ion, 1186.26 amu; found, 1149.51 amu (M – HCl = 1150.28 amu).

5-(3,4-Catecholato(hydrotris(3,5-dimethyl-1-pyrazolyl)borato)oxomolybdenum(V))-10,15,20-tri-*p*-tolylporphinatoiron(III)–Bis(*N*-methylimidazole) Adduct (Fe(*N*-MeIm)$_2$(3,4-Mo-TTP), 13). Compound **13** (~1

(21) Gust, D.; Moore, T. A.; Bensasson, R. V.; Mathes, P.; Land, E. I.; Chachaty, C.; Moore, A. L.; Liddle, P. A. *J. Am. Chem. Soc.* **1985**, *107*, 3631–3640.

(22) LaBarre, M. J. Ph.D. Dissertation, University of Arizona, Tuscon, AZ, 1992.

$\times 10^{-3}$ M) was generated in solution by addition of *N*-methylimidazole ($\sim 1 \times 10^{-1}$ M) to **11** ($\sim 1 \times 10^{-3}$ M). The solvent was DMF, methylene chloride, or methylene chloride–toluene (1:1).

5-(2,3-Catecholato(hydrotris(3,5-dimethyl-1-pyrazolyl)borato)oxomolybdenum(V))-10,15,20-tri-*p*-tolylporphinatoiron(III)–Bis(*N*-methylimidazole) Adduct (Fe(*N*-MeIm)$_2$(2,3-Mo-TTP), 14). Compound **14** was prepared in solution according to the procedure for **13**.

Molecular Modeling. Molecular modeling simulations were performed on a Silicon Graphics IRIS system using the program SYBYL by Tripos Associates, Inc. The lowest energy van der Waals configurations were determined using the SYBYL interactive energy minimization routine MAXMIN2. The coordinates for the porphyrin moiety (TTP) and the molybdenum fragment ([LMoO]$^{3+}$) were obtained from the Cambridge Structural Database. These fragments were combined keeping in mind the approximately octahedal enviornment around the Mo center and using typical Mo–O single bond distances of 1.96 Å. The range of sterically allowed rotations were investigated within the SYBYL graphics package as well as with scale models built to conform to the SYBYL data.

Measurement of Equilibrium Constants. Equilibrium constants were measured from the absorbances of (0.8–1.2) $\times 10^{-3}$ M solutions in a 1-cm pathlength cuvette according to the method described in the literature.[23] Measurements were done with same concentrations (0.8–1.2) $\times 10^{-3}$ M) of iron porphyrins but varying concentrations of *N*-methylimidazole. Plots of $\log[(A - A_0)/(A_c - A)]$ versus $\log$ [*N*-MeIm] gave satisfactorily linear segments of lines. Here A is the absorption at the wavelength of interest, A_0 is the absorption at that wavelength before addition of *N*-methylimidazole, and A_c is the limiting absorbance at the same wavelength in the presence of a large excess of *N*-MeIm. For addition of one mole of base per mole of porphyrin, the equilibrium constant (K_1) was computed from the intercept of the linear portion of the graph, which yielded a slope $\approx$ 1. Similarly, for addition of two moles of base per mole of iron porphyrin, the equilibrium constant (β_2) was calculated from the intercept of the line segment of slope $\approx$ 2.

Results and Discussion

Synthesis and Characterization. Unsymmetrically substituted dihydroxyporphyrins can be prepared by a modification of the synthetic procedure for the preparation of substituted tetraarylporphyrins.[24,25] Thus, 3,4-OMe-TTP (**1**) and 2,3-OMe-TTP (**2**) are formed from the condensation reaction between pyrrole, *p*-tolualdehyde, and the appropriate benzaldehyde in refluxing propionic acid. The desired product can then be isolated in low yield (1–2%) by column chromatography on silica gel. Demethylation of **1** and **2** with boron tribromide[26] in dry dichloromethane proceeds in high yield (90%) to give the desired porphyrins 3,4-OH-TTP (**3**) and 2,3-OH-TTP (**4**) possessing a single pendant catechol function (Scheme 1). The ^{1}H NMR spectra of the bis-substituted free base porphyrins are consistent with their molecular formulations and the presence of only one dimethoxy- or dihydroxy-substituted phenyl ring per molecule.

Reaction of **3** and **4** with LMoO(eth-gly) in toluene at elevated temperature proceeds in high yield to give the desired porphyrins 3,4-Mo-TTP (**7**) and 2,3-Mo-TTP (**8**) with a pendant oxomolybdenum fragment.[27] These complexes can be purified by chromatography on silca gel, are indefinitely stable in air and stable to water, and are unchanged after 3 h in a solution of refluxing DMF. However, the hydrolytic sensitivity of the complexes to HCl at millimolar concentrations necessitated modification of the methods for inserting zinc and iron into the porphyrin rings of **7** and **8**.

Zinc was inserted into the porphyrins by refluxing **7** or **8** in DMF and adding $ZnCl_2$. The bimetallic Mo–Zn complexes Zn(3,4-Mo-TTP) (**9**) and Zn(2,3-Mo-TTP) (**10**) are indefinately stable in air in the solid state. However, their dichloromethane and DMF solutions are unstable to prolonged heating and seem to be photosensitive.

Iron insetion into **7** and **8** is more complicated and requires the strict exclusion of HCl from the reaction mixture and product complexes to avoid hydrolysis of the catecholate ligand from the molybdenyl group. Compounds FeCl(3,4-Mo-TTP) (**11**) and FeCl(2,3-Mo-TTP) (**12**) were prepared by addition of $FeCl_2 \cdot 4H_2O$ to a refluxing mixture of **7** or **8** in dichloromethane–methanol. The crude product was purified by passing a dichloromethane solution down a silica gel column to convert the monomeric **11** or **12** species into the corresponding μ-oxo dimer. Cleavage of the μ-oxo-dimers to the desired chloroiron(III) monomeric species **11** and **12** was achieved by a biphasic reaction in dichloromethane and aqueous 1 M NaCl. These mild reaction conditions prevent the acid hydrolysis of the molybdenum catecholate fragment. The purified bimetallic complexes are indefintely stable to air and water in the solid state and in solution but are very sensitive to HCl.

All of the substituted porphyrins display electronic absorption spectra that are virtually identical in both peak position and intensity to those of TTP and its chloroiron and zinc insertion products (Table 1). The weak d–d transition of the LMoO(catechol) fragment[16,28] is obscured by the much more intense porphyrin and metalloporphyrin absorbances. Addition of excess *N*-methylimidazole to the chloroiron porphyrin complexes **11** and **12** results in spin pairing of the iron(III) center and a shift in the band positions (*vide infra*).

The infrared spectra of the molybdenum-containing compounds exhibit a strong ν(M=O) band at about 940 cm^{-1} and a weak ν(B—H) band near 2540 cm^{-1}, similar to the bands observed in other LMoO(catechol) species.[28] All the modified porphyrins and their metal complexes have been satisfactorily characterized by mass spectrometry, and representative examples have been characterized by elemental analysis.

Proton NMR Spectroscopy. The porphyrin units of compounds **1–14** have been characterized by proton NMR spectra at ambient temperature (21 °C). Of particular interest are the resonances of the pyrrole protons, which are known to be very sensitive reporters of the electronic structure of paramagnetic metalloporphyrin complexes.[29] For compounds **7–10**, the pyrrole protons resonate in the diamagnetic region (δ 8.83–8.95, multiplet) and are not perturbed by the pendant paramagnetic molybdenum

Table 1. Electronic Spectral Data in Toluene at 25 °C

compd	λ, nm ($\epsilon \times 10^{-3}$, L·mol^{-1}·cm^{-1})
1	516 (17.4), 552 (9.33), 594 (5.01), 649 (4.37)
2	516 (19.5), 550 (8.51), 592 (5.37), 652 (5.62)
3	516 (17.8), 551 (9.55), 594 (5.25), 652 (7.59)
4	515 (18.6), 550 (8.71), 592 (6.03), 651 (9.55)
5	508 (12.3), 573 (6.03), 612 (3.47), 655 (2.40), 690 (2.57)
6	509 (12.9), 573 (4.07), 598[b] (3.31), 657 (3.09), 690 (3.55)
7	518 (19.1), 554 (12.6), 595 (5.89), 653 (7.59)
8	516 (18.2), 551 (9.55), 594 (5.37), 652 (7.24)
9	515 (4.47), 552 (24.0), 592 (6.92)
10	513 (3.02), 551 (22.9), 590 (4.90)
11	509 (14.1), 571 (5.50), 693 (3.72)
12	509 (15.1), 573 (4.17), 690 (3.63)
13[a]	556 (7.24), 518[b] (6.61), 644[b] (2.50)
14[a]	555 (7.24), 579 (6.17), 647[b] (1.58)

[a] In DMF. [b] Shoulder.

(23) (a) Walker, F. A.; Lo, M.-W.; Ree, M. T. *J. Am. Chem. Soc.* **1976**, *98*, 5552–5560. (b) Walker, F. A.; Balke, V. L.; West, J. T. *J. Am. Chem. Soc.* **1985**, *107*, 1226–1233.

(24) (a) Little, R. G.; Anton, J. A.; Loach, P. A.; Ibers, J. A. *J. Heterocycl. Chem.* **1975**, *12*, 343–349. (b) Little, R. G. *J. Heterocycl. Chem.* **1981**, *18*, 129–133; 833–834.

(25) Dutta-Gupta, N.; Malakar, D.; Rice, L.; Rivers, S. *J. Heterocycl. Chem.* **1987**, *24*, 629–632.

(26) (a) Chan, A. C.; Dalton, J.; Milgrom, L. R. *J. Chem. Doc., Perkin Trans.* **1982**, 707–710. (b) McOmie, J. F. W.; Watts, M. L.; West, D. E. *Tetrahedron* **1968**, *24*, 2289–2292.

(27) LaBarre, M. J.; Raitsimring, A.; Enemark, J. H. In *Molybdenum Enzymes, Cofactors and Model Systems*; Stiefel, E. I., Coucouvanis, D., Newton, W. E., Eds.; ACS Symposium Series 535; American Chemical Society: Washington, DC, 1993; pp 130–142.

(28) Basu, P.; Li, Z.; Bruck, M.; Dhawan, I.; Enemark, J. H. Submitted for publication.

(29) La Mar, G. N.; Walker, F. A. In *The Porphyrins*; Dolphin, D., Ed.; Academic Press: New York, 1979; Vol. IV, Part B, pp 66–157.

Scheme 1 [a]

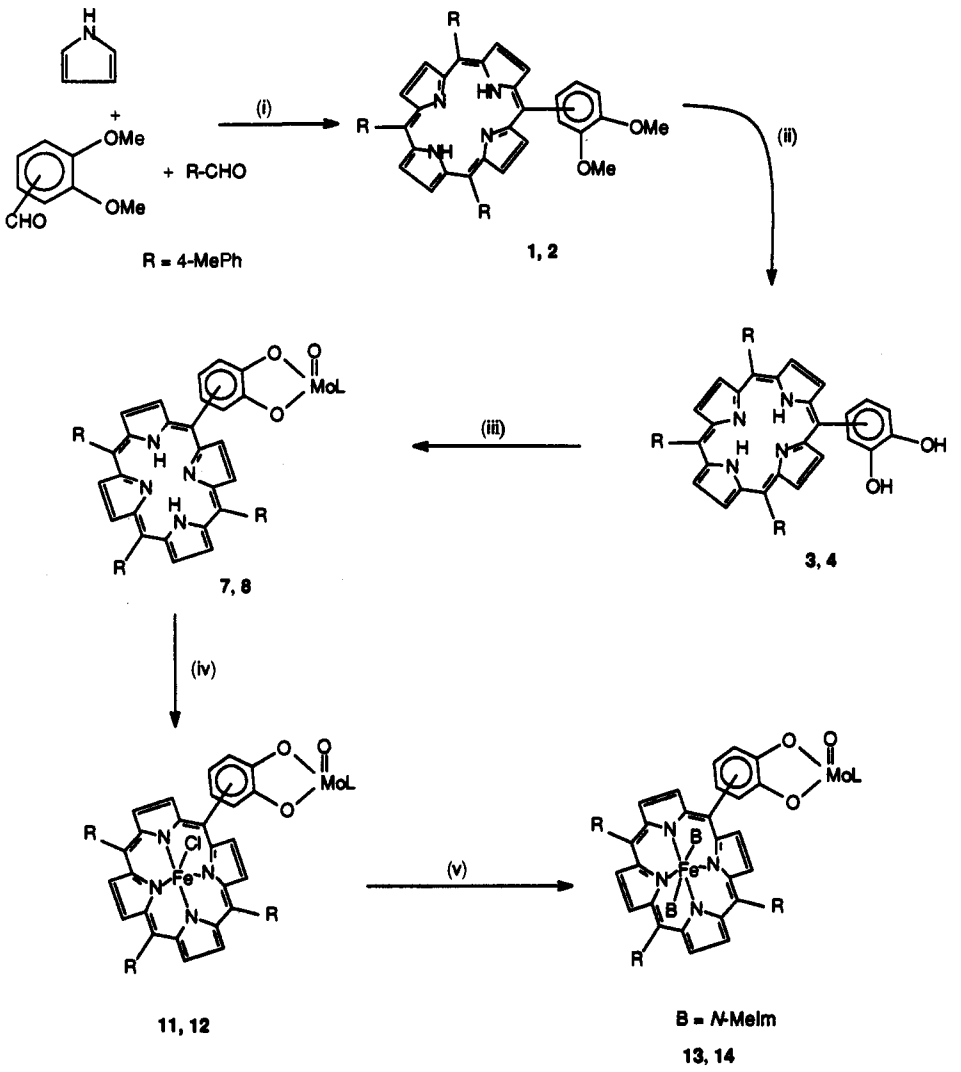

[a] (i) Propionic acid, reflux; (ii) BBr_3, dichloromethane; (iii) LMoO(eth-gly), toluene; (iv) $FeCl_2{\cdot}4H_2O$, dichloromethane–methanol; (v) excess *N*-MeIm.

center. In contrast, the protons of the pyrazolylborate ligand itself are too broad to be interpreted. Compounds **5**, **6**, **11**, and **12** possess high-spin Fe(III) and exhibit broad pyrrole peaks near 80 ppm. Addition of a 5–7-fold excess of *N*-MeIm to a 0.5×10^{-3} mM solution of **11** or **12** yields the respective low-spin Fe(III) complex **13** or **14**, which exhibits distinctive pyrrole resonance patterns centered around −17 ppm. The number of pyrrole protons within these resonances can be quantitated by comparison to the broad signal near 18 ppm due to the six protons of the two *N*-MeIm ligands. For **13**, the eight pyrrole resonances fall into three distinct peaks between −16 and −19 ppm. For **14**, the eight pyrrole protons give rise to seven distinct peaks between −11 and −24 ppm. The large number of observable pyrrole resonances for **14** could be due to hindered rotation of one of the axial *N*-MeIm ligands because of the close proximity of the bulky LMoO(catechol) fragment. Alternatively, the multiple pyrrole resonances may simply reflect the inherent asymmetry introduced into the porphyrin ring system by the nearby LMoO(catechol) fragment.[30] Tempeature-dependent proton NMR experiments are in progress to allow us to better understand the distinctive spectral patterns of the pyrrole protons of **13** and **14**.[31]

Molecular Modeling. All attempts to obtain diffraction quality crystals of any of the modified porphyrins or of their Mo, Fe, or Zn complexes have been unsuccessful. Therefore, molecular modeling calculations have been performed in order to estimate the Mo···M (M = Zn, Fe) distances in **9**–**14**. The strict geometrical constraints of both the TTP and the $[LMoO]^{3+}$ fragments allow the two domains to be constructed from single crystal structural data and then joined together. The bulky methyl groups on the pyrazolylborate ligand and the planar nature of the porphyrin severely limit the structural freedom within these molecules. To a first approximation, the only structural variable in these complexes is rotation about the C–C bond that links the methine carbon of the porphyrin ring to the catecholate group coordinated to the oxo-Mo(V) center. Moreover, during rotation about this bond, the Mo···M vector will trace out part of a cone with a relatively constant Mo···M distance. Ruffling of the porphyrin ring[17] will also have little effect on the Mo···M distance. For compounds **9**, **11**, and **13**, the catechol ring is calculated to lie roughly perpendicular to the central plane of the porphyrin, with Mo···M ~9.4 Å. For **10** and **12**, one of the methyl groups of the pyrazolylborate fragment lies directly above the π-system of the porphyrin plane, and the entire Mo–catechol ring system is twisted more than 30°; the calculated Mo···M distance for **10** and **12** is 7.3 Å. For **14**, the calculated Mo···Fe distance is 7.9 Å. Figure 3 shows the calculated structures for **13** and **14**.

(30) Walker, F. A.; Simonis, U.; Zhang, H.; Walker, J. M.; Ruscitti, T. M.; Kipp, C.; Amputch, M. A.; Castillo, B. V., III; Cody, S. H.; Wilson, D. L.; Graul, R. E.; Young, G. J.; Tobin, K.; West, J. T.; Barichievich, B. A. *New J. Chem.* **1992**, *16*, 609–620.

(31) Basu, P.; Walker, F. A.; Enemark, J. H. Unpublished results.

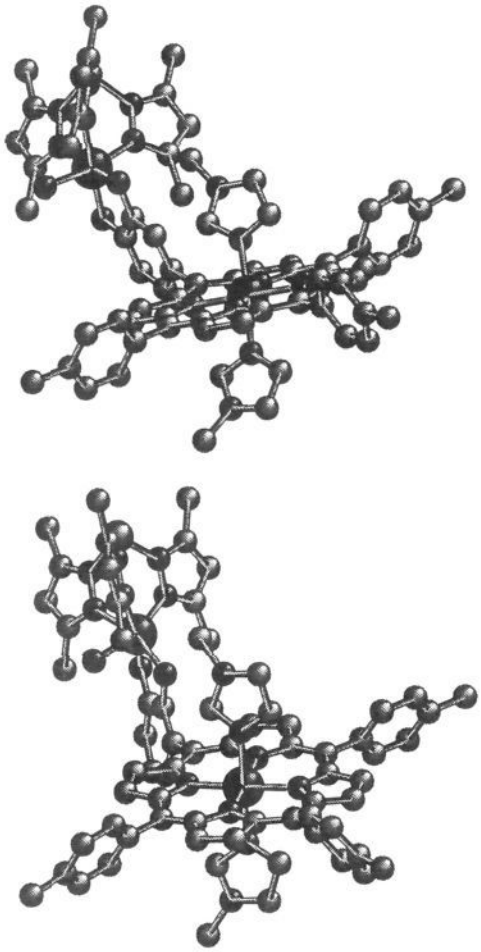

Figure 3. Calculated geometry of **13** (a, top) and **14** (b, bottom).

Determination of the Formation Constants. The nature and extent of the transmission of electronic effects from the porphyrin periphery to the four nitrogen atoms (and thereby to the inserted metal) has been an active field of research in metalloporphyrin chemistry.[20,32-45] The electronic effects of the groups attached to the porphyrin periphery can be directly transmitted to the core nitrogens because of the conjugated nature of the porphyrin ring. Peripheral groups have been shown to affect the redox properties, absorption spectra, and the rates and equilibrium constants for the addition of axial ligands. For tetraarylporphyrins the changes in these properties can be correlated with the Hammett σ constants of the peripheral substituents. It is also known that these properties show different dependencies for symmetrically and unsymmetrically meso-substituted porphyrins.[20,23b,46,47]

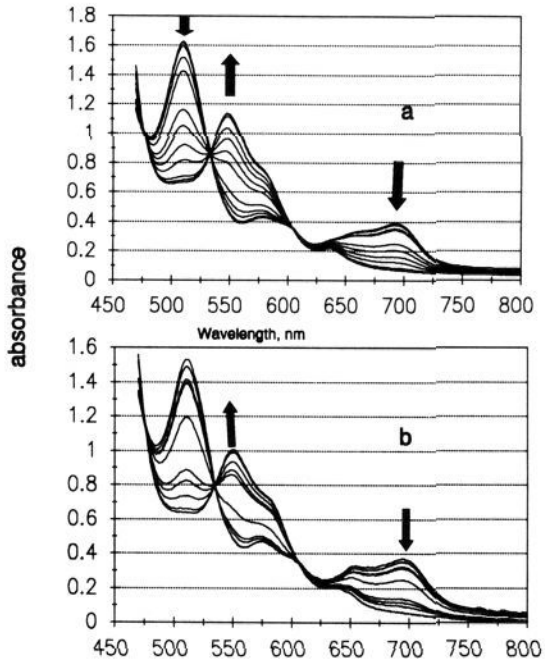

Figure 4. Spectral changes observed when *N*-MeIm is added to **5** (a) and **12** (b).

Table 2. Equilibrium Constants for Addition of *N*-MeIm to Fe(III) Porphyrins[a]

compd	K,[b] M^{-1}	$\beta_2 \times 10^{-4}$, M^{-2}
Fe(TPP)Cl[c]	88 ± 12	1 ± 0.2
5	116 ± 4	1.26 ± 0.15
6	98 ± 40	2.06 ± 0.28
11	189 ± 15	3.94 ± 0.14
12	209 ± 86	7.54 ± 0.78

[a] Conditions: solvent, dichloromethane; temperature, 298 K; concentration, (0.8–1.2) × 10^{-4} M. [b] Obtained by assuming that the extinction coefficients for the mono- and bis-adducts are the same, ref 23a. [c] Value taken from ref 23.

Figure 4 shows the spectral changes and tight isosbestic points that are observed when *N*-methylimidazole is added to the Fe(III) complexes of the unsymmetrically substituted porphyrins described above. The equilibrium constants for coordination of

(32) Meot-Ner, M.; Adler, A. D. *J. Am. Chem. Soc.* **1972**, *94*, 4763–4764; **1975**, *97*, 5107–5111.
(33) Quimbly, D. J.; Longo, F. R. *J. Am. Chem. Soc.* **1975**, *97*, 5111–5117.
(34) (a) Kadish, K. M.; Bottomley, L. A. *J. Am. Chem. Soc.* **1977**, *99*, 2380–2382. (b) Kadish, K. M.; Morrison, M. M. *Bioinorg. Chem.* **1977**, *7*, 107–115.
(35) (a) Walker, F. A.; Hui, E.; Walker, J. M. *J. Am. Chem. Soc.* **1975**, *97*, 2390–2397. (b) Walker, F. A. *J. Am. Chem. Soc.* **1973**, *95*, 1150–1153; 1154–1159. (c) Walker, F. A.; Beroiz, D.; Kadish, K. M. *J. Am. Chem. Soc.* **1976**, *98*, 3484–3489. (d) McDermott, G. A.; Walker, F. A. *Inorg. Chim. Acta* **1984**, *91*, 95–102. (e) Walker, F. A.; Balke, V. L.; McDermott, G. A. *Inorg. Chem.* **1982**, *21*, 3342–3348. (f) Walker, F. A.; Balke, V. L.; McDermott, G. A. *J. Am. Chem. Soc.* **1982**, *104*, 1569–1574. (g) Walker, F. A.; Benson, M. *J. Phys. Chem.* **1982**, *86*, 3495–3499. (h) Walker, F. A. *J. Am. Chem. Soc.* **1970**, *92*, 4235–4244. (i) Walker, F. A.; Reis, D.; Balke, V. L. *J. Am. Chem. Soc.* **1984**, *106*, 6888–6898.
(36) (a) Baker, E. W.; Storm, C. B.; McGrew, G. T.; Corwin, A. H. *Bioinorg. Chem.* **1973**, *3*, 49–60. (b) Storm, C. B.; Teklu, Y. *J. Am. Chem. Soc.* **1972**, *94*, 1745–1747.
(37) Jones, R. D.; Summerville, D. A.; Basolo, F. *J. Am. Chem. Soc.* **1978**, *100*, 4416–4424.
(38) (a) Caughey, W. S.; Deal, R. M.; McLees, B. D.; Alben, J. O. *J. Am. Chem. Soc.* **1962**, *84*, 1735–1736. (b) Caughey, W. S.; Fujimoto, W. Y.; Johnson, B. P. *Biochemistry* **1966**, *5*, 3830–3843. (c) McLees, B. D.; Caughey, W. S. *Biochemistry* **1968**, *7*, 642–652.
(39) (a) Higginbotham, E.; Hambright, P. *Inorg. Nucl. Chem. Lett.* **1972**, *8*, 747–750. (b) Worthington, P.; Hambright, P.; Williams, R. F. X.; Feldman, M. R.; Smith, K. M.; Langry, K. C. *Inorg. Nucl. Chem. Lett.* **1980**, *46*, 441–447. (c) Worthington, P.; Hambright, P.; Williams, R. F. X.; Reid, J.; Burnham, C.; Shamin, A.; Turay, J.; Bell, D. M.; Kirkland, R.; Little, R. G.; Datta-Gupta, N.; Eisner, U. *J. Inorg. Biochem.* **1980**, *12*, 281–291. (d) Williams, G. N.; Hambright, P. *Inorg. Chem.* **1978**, *17*, 2687–2688. (e) Kirksey, C. H.; Hambright, P.; Storm, C. B. *Inorg. Chem.* **1969**, *8*, 2141–2144. (f) Dhears, B.; Shah, B.; Hambright, P. J. *J. Am. Chem. Soc.* **1971**, *93*, 776–778. (g) Reid, J. B.; Hambright, P. *Inorg. Chem.* **1977**, *16*, 968–969.
(40) Vogel, G. C.; Beckman, B. A. *Inorg. Chem.* **1976**, *15*, 483–484.
(41) (a) Eaton, S. S.; Eaton, G. R. *J. Am. Chem. Soc.* **1977**, *99*, 1601–1604. (b) Eaton, S. S.; Fishwild, D. M.; Eaton, G. R. *Inorg. Chem.* **1978**, *17*, 1542–1545. (c) Eaton, S. S.; Eaton, G. R. *J. Am. Chem. Soc.* **1977**, *99*, 6594–6599.
(42) Rillema, D. P.; Nagle, K. J.; Barringer, L. F.; Meyer, T. J. *J. Am. Chem. Soc.* **1981**, *103*, 56–62.
(43) Hagen, K. I.; Schwab, C. M.; Edwards, J. O.; Jones, J. G.; Lawler, R. G.; Sweigert, D. A. *J. Am. Chem. Soc.* **1992**, *114*, 6930–6931.
(44) Toney, G. E.; Gold, A.; Savrin, J.; ter Harr, L. W.; Sangaiah, R.; Hatfield, W. E. *Inorg. Chem.* **1984**, *23*, 4350–4352.
(45) (a) Bottomley, L. A.; Kadish, K. M. *Inorg. Chem.* **1981**, *20*, 1348–1357. (b) Kadish, K. M.; Bottomley, L. A.; Beroiz, D. *Inorg. Chem.* **1978**, *17*, 1124–1129.
(46) Walker, F. A.; Balke, V. L.; McDermott, G. A. *J. Am. Chem. Soc.* **1982**, *104*, 1569–1574.
(47) Walker, F. A.; Barry, J. A.; Balke, V. L.; McDermott, G. A.; Wu, M. Z.; Linde, P. F. *Adv. Chem. Ser.* **1982**, *201*, 377–416.

Table 3. Cyclic Voltammetric Data in DMF at 25 °C[a]

	$E_{1/2}$,[c] V (ΔE_p,[d] mV)			
	$Mo^{V/IV}$	$Fe^{III/II}$	$Fe^{II/I}$	$P^{0/-}$ [b]
5		−0.268;[e] −0.113[f]	1.081 (59)	−1.704 (63)
6		−0.286;[e] −0.156[f]	−1.088 (67)	−1.715 (75)
FeClTTP		−0.267;[e] −0.130[f]	−1.080 (66)	−1.673 (74)
Fe(*N*-MeIm)$_2$TTPCl[g]		−0.130 (69)	−1.442;[e] −1.247[f]	−1.665 (73)
LMoO(catechol)	−0.734 (64)			
7	−0.717 (68)			−1.234 (74)
8	−0.716 (67)			−1.228 (58)
9	−0.698 (69)			−1.438 (60)
10	−0.736 (63)			−1.514 (67)
11	−0.717 (75)	−0.269;[e] −0.187[f]	−1.147 (75)	−1.724 (72)
12	−0.735 (60)	−0.290;[e] −0.129[f]	−1.199 (63)	−1.81 (104)
13[g]	−0.730 (63)	−0.142 (57)	−1.459;[e] −1.271[f]	−1.731 (88)
14[g]	−0.764 (67)	−0.136 (62)	−1.473;[e] −1.324[f]	−1.80 (115)

[a] Conditions: v = 100 mV/s; supporting electrolyte, 0.1 M TEAP; working electrode, glassy carbon; potentials referenced to SCE, calibrated against ferrocene (+0.465 vs SCE) but uncorrected for junction contribution. [b] This porphyrinic response has also been ascribed as the Fe(I/0) reduction for iron porphyrins.[58] [c] $E_{1/2} = 0.5(E_{pa} + E_{pc})$, where E_{pa} and E_{pc} are anodic and cathodic peak potentials, respectively. [d] $\Delta E_p = E_{pc} - E_{pa}$. [e] E_{pc}. [f] E_{pa}. [g] *N*-MeIm concentration, ~0.1 M.

N-methylimidazole were determined by monitoring the absorbance changes at three different wavelengths (Table 2). The equilibrium constants (β_2) for Fe(III) porphyrins that possess a pendant oxomolybdenum fragment FeCl(3,4-Mo-TTP) (**11**) and FeCl(2,3-Mo-TTP) (**12**) are considerably larger than those for Fe(III) complexes of the asymmetric precursor porphyrins (e.g., FeCl(3,4-OMe-TTP) (**5**) and FeCl(2,3-OMe-TTP) (**6**)). A possible origin of this result is discussed in the next section.

Electrochemistry. The redox properties of all the compounds have been examined by cyclic voltammetry in DMF solution at a glassy carbon electrode at 25 °C (scan rate 100 mV/s). All potentials were calibrated with respect to the ferrocenium/ferrocene couple and referenced to the saturated calomel electrode (SCE). The half-wave potentials are listed in Table 3, and representative voltammograms are shown in Figures 5 and 6. All complexes exhibit pseudo-Nernstian one-electron reductions as demonstrated by $i_{pa}/i_{pc} \approx 1.0$ for all of the redox processes except the high-spin Fe(III/II) and low-spin Fe(II/I) couples. For the former couple, a single cathodic process is observed during the negative potential sweep, but a broad peak is seen on scan reversal. The more cathodic process is assigned to the $Fe^{III}Cl(TTP)/[Fe^{II}Cl(TTP)]^-$ reduction. The $[Fe^{II}Cl(TTP)]^-$ anion is known to lose chloride readily,[45,48] and therefore the broad anodic process is probably due to $Fe^{II}(TTP)/[Fe^{III}(TTP)]^+$ oxidation. Upon addition of coordinating bases, both the Fe(III) and the Fe(II) centers become low-spin, and the iron(III/II) couples become nicely reversible and are shifted to more positive potentials. The Fe(III/II) reduction potential of the low-spin Fe(III) complexes varies from −0.130 to −0.142 V (vs SCE). This relatively small range of reduction potentials has been ascribed to the insensitivity of the $d_{xz,yz}$ acceptor orbitals of a low-spin d^5 electron configuration to unsymmetrical meso substitution on the porphyrin skeleton.[47]

For high-spin Fe(III), on the other hand, the d_{xy} orbital in the plane of the porphyrin ring is the acceptor orbital, and therefore the high-spin Fe(III)/(II) couple is more sensitive to the inductive effect of the meso position.[47] The comparison of the Fe(III)/(II) couples for high-spin complexes is restricted to the cathodic wave because of chloride dissociation from the $[Fe^{II}Cl(TTP)]^-$ anion (*vide supra*). The Fe(III/II) reductions for **5** and **11** occur at the same potential. Relative to the **5**, **11** pair, the **6** and **12** pair is also isopotential but is shifted cathodically by ~20 mV. The Fe(III/II) reduction for FeCl(TTP) is observed at the same potential as **5** and **11**. The similarity of the potentials of **5** and FeCl(TTP) can be explained by comparison of their effective Hammett σ-constants.[49,50]

For the Fe(II/I) reduction, the electron goes into the d_{z^2} orbital for the low-spin case; for the high-spin case, the electron is believed to go into the $d_{xz,yz}$ orbital with subsequent reorganization occurring so that the unpaired electron resides in the d_{z^2} orbital.[51,52] The d_{z^2} orbital has a small ring of electron density in the porphyrin plane, and the Fe(II/I) reduction is less sensitive to meso substitution than is the high-spin Fe(III/II) couple. The Fe(II/I) potentials for **5**, **6**, and FeCl(TTP) are essentially the same, probably because of the relatively small difference in electron-donating/withdrawing properties among these porphyrin systems. For **11**–**14**, the Fe(II/I) reduction is preceded by a molybdenum(V/IV) reduction, which makes the unsymmetrical ring more electron-donating and thereby shifts the Fe(II/I) couple to more negative potentials relative to FeCl(TTP) and Fe(*N*-MeIm)$_2$(TTP)Cl. The Fe(II/I) potentials of **13** and **14** will also be affected by their respective formation constants in the two oxidation states.[48] Low-spin iron(II) loses axial ligands upon reduction.[45,52,53] Therefore, the Fe(II/I) couples of Fe(*N*-MeIm)$_2$(TTP)Cl, Fe(*N*-MeIm)$_2$(3,4-Mo-TTP)Cl (**13**), and Fe(*N*-MeIm)$_2$(2,3-Mo-TTP)Cl (**14**) are not completely reversible and depend linearly upon the *N*-MeIm concentration. However, at very low temperature, binding of one axial ligand to Fe(I) has been observed.[54] At more negative potentials, **11**–**14** show reduction waves (Table 3) that can be assigned either to porphyrin reductions[55–57] or to Fe(I/0) reduction.[58]

The oxomolybdenum centers show a reversible reduction near −0.7 V (vs SCE). The one-electron nature of the reductions was confirmed from comparison of the current height to that in other LMoO(X,Y) complexes.[16,59] The Mo(V/IV) couple of LMoO(catechol) complexes is sensitive to substitutions on the catechol ring. For LMoO(catechol) itself, the Mo(V/IV) reduction occurs

(48) Kadish, K. M. In *Iron Porphyrins*, Part II; Lever, A. B. P., Gray, H. B., Eds.; Addison-Wesley Publishing Co.: Massachusetts, 1983; pp 161–249.
(49) Jaffe, H. H. *Chem. Rev.* **1953**, *53*, 191–261.
(50) For **5**, the σ-constants of the *m*-OMe(0.115) and *p*-OMe(−0.268) groups sum to −0.153, a value close to the σ-constant for *p*-Me (−0.170).
(51) Cohen, I. A.; Ostfeld, D.; Litchtenstein, B. *J. Am. Chem. Soc.* **1972**, *94*, 4522–4525.
(52) Lexa, D.; Momenteau, M.; Mispelter, J. *Biochim. Biophys. Acta* **1974**, *338*, 151–163.
(53) Lexa, D.; Momenteau, M.; Mispelter, J.; Lhoste, J. M. *Bioelectrochem. Bioenerg.* **1975**, *1*, 108–117.
(54) (a) Srivasta, G. S.; Sawyer, D. T.; Boldt, N. J.; Bocian, D. F. *Inorg. Chem.* **1985**, *24*, 2123–2125. (b) Donohoe, R. J.; Atamian, M.; Bocian, D. F. *J. Am. Chem. Soc.* **1987**, *109*, 5593–5599.
(55) Kadish, K. M.; Larson, G.; Lexa, D.; Momenteau, M. *J. Am. Chem. Soc.* **1975**, *97*, 282–288.
(56) Kadish, K. M.; Morrison, M. M.; Constant, L. A.; Dickens, L.; Davis, D. G. *J. Am. Chem. Soc.* **1976**, *98*, 8387–8390.
(57) Giraudeau, A.; Callot, H. J.; Jordan, J.; Ezhar, I.; Gross, M. *J. Am. Chem. Soc.* **1979**, *101*, 3857–3862.
(58) Lexa, D.; Saveant, J. M. In *Redox Chemistry and Interfacial Behavior of Biological Molecules*; Dryhurst, G., Niki, K., Eds.; Plenum: New York, 1988; pp 1–25.
(59) (a) Chang, C. S. J.; Enemark, J. H. *Inorg. Chem.* **1991**, *30*, 683–688. (b) Chang, C. S. J.; Collison, D.; Mabbs, F. E.; Enemark, J. H. *Inorg. Chem.* **1990**, *29*, 2261–2267. (c) Chang, C. S. J.; Rai-Chaudhuri, A.; Lichtenberger, D. L.; Enemark, J. H. *Polyhedron* **1990**, *9*, 1967–1973.

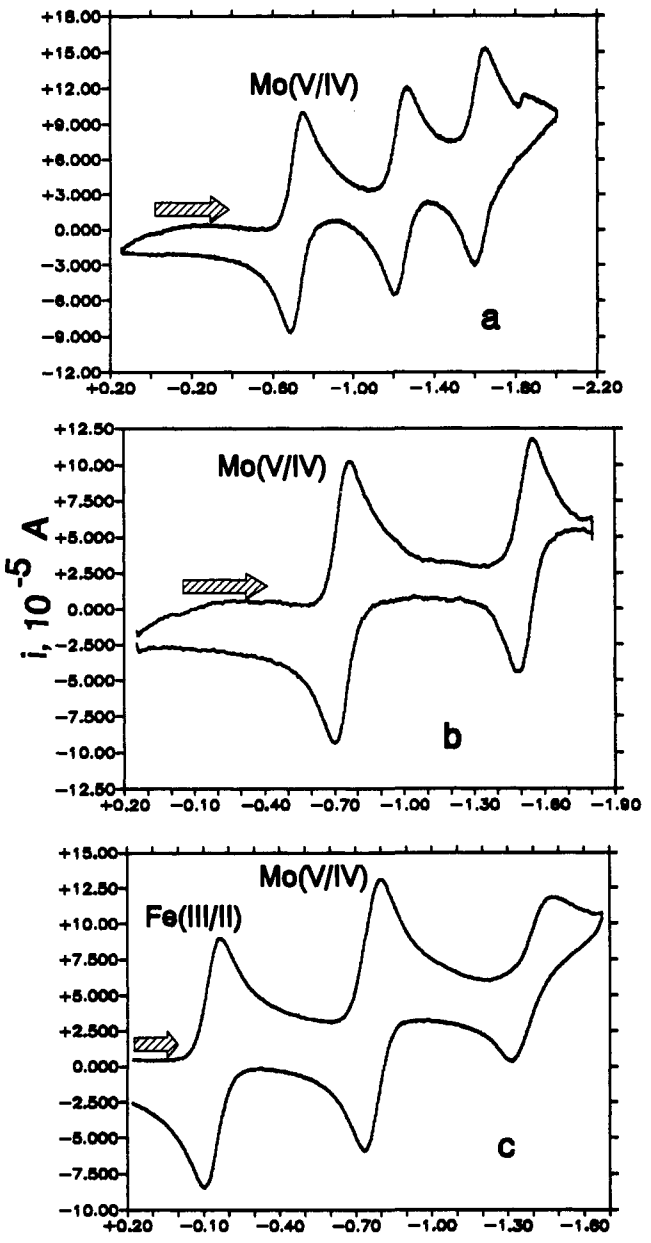

Figure 5. Cyclic voltammograms of **8** (a), **10** (b), and **14** (c) in DMF solution (1 mM) at 25 °C. Scan rate, 100 mV s^{-1}; *N*-MeIm concentration, ~ 0.1 M.

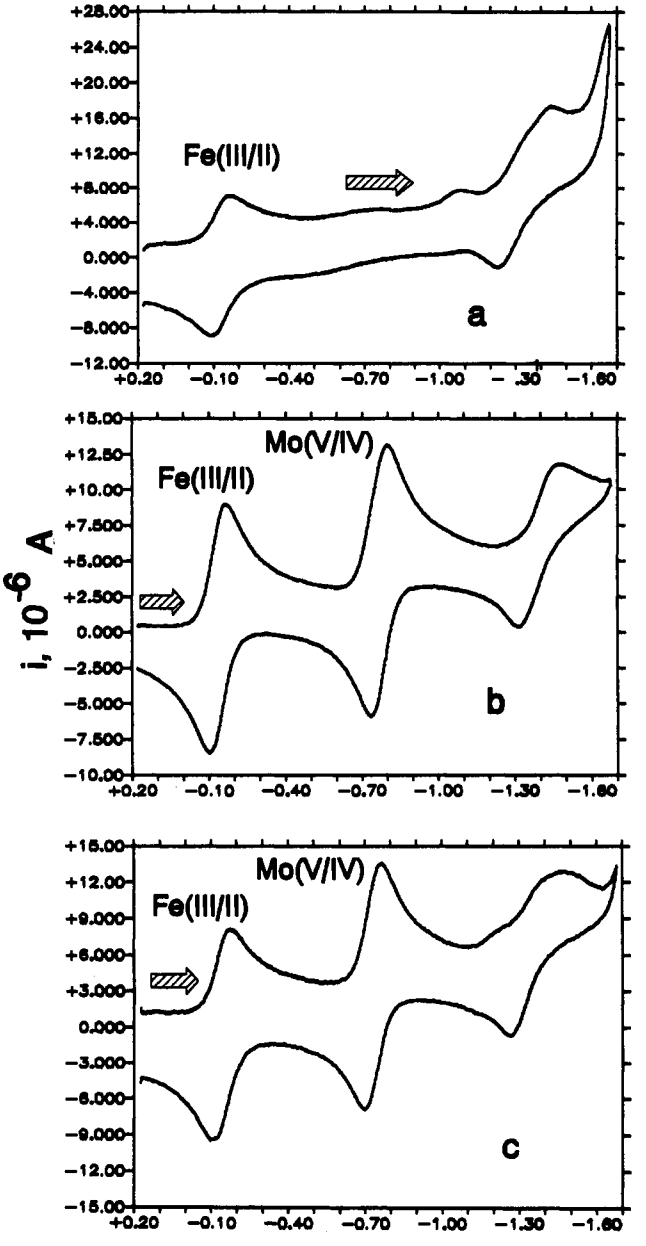

Figure 6. Cyclic voltammograms of Fe(*N*-MeIm)$_2$(TTP)Cl (a), **14** (b), and **13** (c) in DMF solution (1 mM) at 25 °C. Scan rate, 100 mV s^{-1}; *N*-MeIm concentration, ~ 0.1 M.

at −0.734 V; for **7** and **8**, in which the catechol ring is attached to the porphyrin ring system, the Mo(V/IV) potential is −0.717 V. The potentials of **7** and **8** behave differently upon metalation of their porphyrin centers. Metalated complexes derived from **8** are more cathodically shifted than those derived from **7**. Comparison of the potentials for all of the Mo···Fe complexes (**11**–**14**) shows that the Mo(V/IV) potentials shift cathodically when the iron center changes from high-spin to low-spin and that the shift is larger for the **12**/**14** pair than for the **11**/**13** pair. The cyclic voltammetry results clearly show that the potential of the Mo(V/IV) couple is sensitive to events occurring at the porphyrin core, including metal insertion, type of metal, and electronic configuration of the metal.

The formation constant data in Table 2 show that the bis-*N*-methylimidazole adduct of **6** is about 1.6 times more stable than **5**. Likewise, β_2 for **12** is 1.9 times larger than that for **11**. The higher stability constant of **6** compared to **5** can be explained by the electron-donating effect of the unsymmetrically substituted meso position. The larger effective σ-constant for **6** compared to **5** is also evidenced by the more cathodic Fe(III/II) redox peak. More electron-donating groups tend to neutralize the formal positive charge on low-spin Fe(III) and thereby stabilize the adduct (higher formation constant).[23,60a] The same reasoning probably accounts in part for **12** having β_2 ~1.9 times greater than that of **11**.

It is interesting to note that β_2 for **11** is about 3.1 times greater than that for **5** although their Fe(III/II) couples are isopotential. Likewise, β_2 for **12** is about 3.7 times that for **6**, its isopotential partner. Relatively larger formation constants for complexes of sterically hindered porphyrins and axial bases have been reported previously[61-63] and explained in terms of a so-called ortho effect.[61]

(60) (a) Sartterlee, J. D.; La Mar, G. N.; Frye, J. S. *J. Am. Chem. Soc.* **1976**, *98*, 7275–7282. (b) Sartterlee, J. D.; La Mar, G. N.; Bold, T. J. *J. Am. Chem. Soc.* **1977**, *99*, 1088–1093.

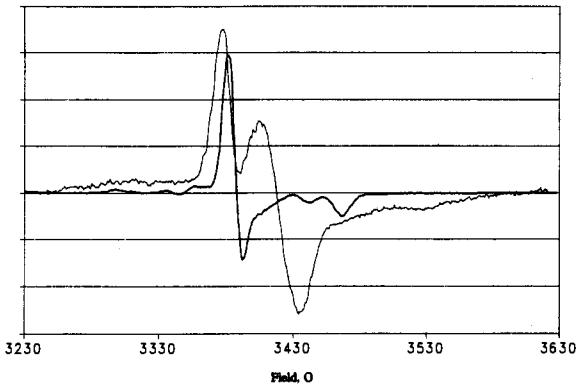

Figure 7. EPR spectra of **9** (bold line) and **13** (light line) in 1:1 dichloromethane–toluene glass, 77 K. Conditions: frequency, 9.2693 GHz; power, 0.2 mW; modulation, 1 G; gain, 1×10^5; sweep time, 335.54 s.

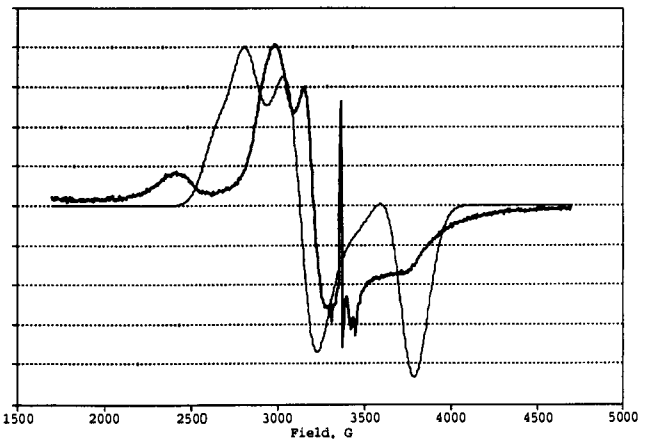

Figure 8. Experimental (bold line) and simulated (light line) spectra of **14**. Experimental conditions: frequency, 9.2803 GHz; power, 0.2 mW; modulation, 5.7 G; gain 1×10^5; sweep time, 671.099 s. Simulation was done with an exchange interaction $J/h = 12$ GHz (0.4 cm^{-1}). The sharp signal at ~3400 G in the experimental spectrum is due to the presence of a minor mononuclear Mo(V) impurity (~0.1%).

For **13** and **14**, molecular modeling calculations show that the methyl groups of the axial *N*-MeIm ligand and one of the methyl groups of the pyrazolylborate ligand can approach within the van der Waals contact (~4 Å) of one another. Weak attractions between these groups may account for the relatively larger formation constants for these compounds.

The results presented in this selection have shown that the properties of the two individual metal centers in these bimetallic systems are only slightly perturbed by one another. This weak interaction has been probed in more detail by EPR spectroscopy (*vide infra*).

EPR Spectra. The isotropic X-band solution EPR spectra of **7** and **8** are typical for LMoO(catechol) complexes ($\langle g \rangle = 1.953$, $A(^{95,97}\text{Mo}) = 39 \times 10^{-4}$ cm^{-1}).[16,28] AT 77 K, these complexes display nearly axial spectra due to the pseudo-3-fold axis formed by the three nitrogen atoms of the facially coordinated tris(pyrazolyl)borate ligand and the oxygens of the oxo and catecholato ligands which make up another facially coordinating ligand set. The EPR spectra of **9** and **10**, which have Zn(II) coordinated by the porphyrin center, are essentially identical to those of the unmetalated complexes, **7** and **8**.

Complexes **11** and **12**, which possess both Mo(V) and high-spin Fe(III) centers, show a broad EPR signal around $\langle g \rangle = 6$ that is typical of high-spin Fe(III) porphyrins and a signal near $\langle g \rangle = 2$ for Mo(V). The positions of these two EPR signals are not detectably different from those of the appropriate monometalated species, but the intensity of the molybdenum signal is greatly reduced due to dipolar coupling with the rapidly relaxing iron center.[27]

Dipolar coupling is highly dependent upon the distance between the two paramagnetic centers. The dipole–dipole interaction in **12**, which has a calculated Mo···Fe distance of 7.3 Å, should be about twice as large as that for **11**, which has a calculated Mo···Fe distance of 9.4 Å, assuming other conditions are nearly identical. Intensity measurements corrected for concentration indicate that only about 20% of the EPR intensity of the Mo(V) signal of **8** remains after metalation with Fe(III) to form **12**, whereas approximately 45% of the Mo(V) signal of **7** is present after it has been metalated with Fe(III) to give **11**.[27] These intensity changes with distance are consistent with the predictions of the simplified theory.

Addition of excess *N*-methylimidazole to **11** or **12** leads to spin pairing of the Fe(III) center ($S = {}^1/_2$) and more complex coupling behavior in the EPR spectra. Figure 7 compares the Mo(V) portions of the EPR spectra of Zn(3,4-Mo-TTP) (**9**) and Fe(*N*-MeIm)$_2$(3,4-Mo-TTP) (**13**). In the coupled system **13**, the spectrum is transformed into a doublet, with the components separated by approximately 50 G. Double integration of the entire EPR spectrum of **13** (taking into account the *g*-dependence of the transition probability) shows that, within the limits of experimental error of integration (20%), the EPR spectrum arises from equal amounts of Mo(V) and Fe(III). The EPR spectrum of **13** can be qualitatively explained by assuming that the observed splitting of 50 G (Figure 7) is due to dipolar interaction between the Mo(V) center and the low-spin Fe(III) center. The distance dependence of this dipolar interaction is given by eq 1, where **g**

$$R_{12} = (\alpha g \mu_\beta / \text{splitting})^{1/3} \qquad (1)$$

is the *g*-value of Fe(III), μ_β is the Bohr magneton, and α is a geometrical factor that depends upon the relative orientations of the paramagnetic centers and which can vary between 0 and 3. Taking the average *g*-value for low-spin Fe(III) as 2.3 and $\alpha = 1.5$, $R_{12} \approx 9$ Å, similar to the intermetal distance obtained from molecular modeling calculations. No splitting is observed in the Fe(III) portion of the spectrum because the line width (~100 G) of typical low-spin Fe(III) complexes is larger than the dipolar splitting. More detailed information about the relative arrangement of the two components of this coupled system may be obtained from spectral simulation (*vide infra*).

A quite different EPR spectrum is obtained for **14** (Figure 8). For **14**, it is still possible to observe the individual components of Fe(III) and Mo(V) in the spectrum, but both signals exhibit broadening of the lines and shifts of the line positions. The molecular modeling calculations for **14** give a Mo···Fe distance of 7.9 Å, and from eq 1, a dipolar interaction of ~90 G is evalulated for this distance. This interaction is still within the EPR line width of Fe(III) and should not noticeably affect the Fe(III) part of the spectrum. The Mo(V) part of the spectrum should be similar to that for **13** but with a large dipolar splitting. However, the EPR spectrum of **14** (Figure 8) does not show the appearance expected for simple dipolar splitting, and a complete explanation of the spectral features of **14** requires that the exchange interaction between the two metal centers be taken into account. It is well known that if the exchange energy is equal to or larger than the Zeeman energy, then the individual spectral features of the two metal centers will disappear,[64,65] as shown in Figure 8, for the calculated spectrum with $J/h = 12$ GHz (0.4 cm^{-1}). In this

(61) Portela, C. F.; Magde, D.; Traylor, T. G. *Inorg. Chem.* **1992**, *32*, 1313–1320.
(62) Nakamura, M. *Inorg. Chim. Acta* **1989**, *161*, 73–80.
(63) Nesset, M. J. M. Ph.D. Thesis, University of Arizona, Tuscon, AZ, 1993.
(64) Pilbrow, J. R. *Transition Ion Electron Paramagnetic Resonance*; Oxford University Press: New York, 1990.

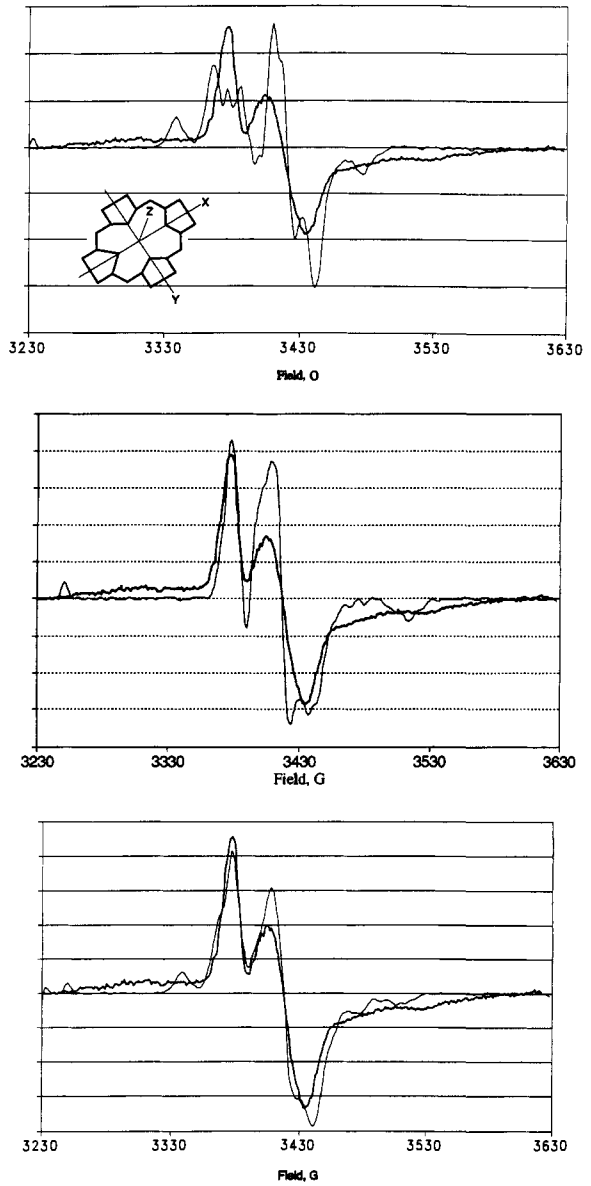

Figure 9. Experimental (bold line) and simulated (light line) EPR spectra of **13** in 1:1 dichloromethane–toluene glass (77 K). Experimental conditions: frequency, 9.2693 GHz; power, 0.2 mW; modulation, 1 G; gain 1×10^5; sweep time, 335.54 s. (a, top) Axis is set as shown, (b, middle) rotation about z-axis by 45°, (c, bottom) summation of simulated spectra in three orientations (0°, 45°, and 50°) with equal weight.

rhombic-like EPR spectrum, the principle g-values are averages of the corresponding g-values of the Fe(III) and Mo(V) centers. The experimental EPR spectrum of **14** (Figure 8) still contains the individual features of each metal center; therefore, for **14**, $J/h < 12$ GHz (0.4 cm^{-1}). On the other hand, the observed shifts of the peaks of the EPR spectrum require that the exchange interaction be comparable to at least half of the difference in Zeeman energies of Fe(III) and Mo(V), i.e., $J/h > 1$ GHz (0.03 cm^{-1}). Spectral simulation improves upon this simple estimation of the magnitude of the exchange interaction (*vide infra*).

Simulation of the coupled EPR spectra of low-spin Fe(III) and Mo(V) was performed numerically by the Monte-Carlo method[66,67] using the spin-Hamiltonian (eq 2) for a

$$H = \mu_\beta \mathbf{B} \mathbf{g}_1 S_1 + \mu_\beta \mathbf{B} \mathbf{g}_2 S_2 + H_{dd} + H_{exch} \qquad (2)$$

coupled system containing two paramagnetic centers with spins S_1 and S_2 equal $^1/_2$. **B** is the vector of the magnetic field; $\mathbf{g}_1$ and $\mathbf{g}_2$ are g-tensors of the first and second spins in the same coordinate frame. H_{dd} is the part of the Hamiltonian responsible for dipole–dipole interaction (eq 3); r is the vector connecting the two paramagnetic centers and $|r| = R_{12}$, the distance between the centers. The part of the Hamiltonian corresponding to the exchange interaction (H_{exch}) was taken as JS_1S_2, where J is a value of the exchange interaction.

$$H_{dd} = \frac{\mu_\beta^2(\mathbf{g}_1 S_1)(\mathbf{g}_2 S_2)}{R_{12}^3} - 3\frac{\mu_\beta^2\{(\mathbf{g}_1 S_1)\mathbf{r}\}\{(\mathbf{g}_2 S_2)\mathbf{r}\}}{R_{12}^5} \qquad (3)$$

Simulation of the spectra of coupled systems requires a model geometry for description of the dipole–dipole interaction and determination of the exchange interaction (J) which is, in general, undefined. Initially, the simulations were performed with J = 0 in order to minimize the number of variable parameters. Subsequent comparison of experimental and simulated spectra gave an idea of the importance of the exchange term in the Hamiltonian. The reference coordinate frame (RCF) was related to the Fe(III) ion and coincided with the principle axes of the g-tensor of Fe(III), $\mathbf{g}_1$ in eq 1. The z axis of the RCF was perpendicular to the plane of the porphyrin ring. The position of the x,y axes is uncertain.[68] The most probable directions of the x,y axes are along the Fe–N bonds or bisecting the FeN_2 angle.[68] In the calculations, the angle δ between x (or y) and the corresponding Fe–N bond in the RCF was varied from 0° to 90° (Figure 9). Experiments with the analogous Zn-containing porphyrins have shown that the g-tensor of the Mo(V) center has axial symmetry. The g_z-component of the tensor was directed along Mo=O bond. The atomic coordinates from the molecular modeling results were used to determine directional cosines of r, the value of $|R_{12}|$, and the matrix **T** that transforms the Mo(V) $\mathbf{g'}_2$ tensor from the Mo coordinate frame to the RCF as $\mathbf{g}_2 = \mathbf{T}\mathbf{g'}_2\mathbf{T}^{-1}$.

Figure 9 depicts the simulated spectrum of **13**, where the x,y axes of the RCF were directed along Fe–N bonds (δ = 0°). The immediate conclusion which follows from comparison of the experimental and simulated spectra is that the range of the dipole–dipole interaction is sufficient to cover the observed experimental splitting and there is no need to include the exchange interaction in the simulation. However, in this particular case, the simulated spectrum revealed additional peaks at high and low field which were not observed in the experimental spectrum. Figure 9b depicts the simulated spectra with δ = 45°. This simulated spectrum more closely approximates the experimental one. The line positions are nearly coincident, but differences are observed in the intensities. A number of other simulations with various δ were also tested. The best fit was obtained by summing over three orientations of RCF (δ = 0°, 45°, 55°) having equal weight. This simulated spectrum is shown in Figure 9c. Although it is clear that this simulation is not unique, the following conclusions may be drawn. (1) The exchange term in **13** is substantially smaller than dipole–dipole interaction and ought to be on the order of the line width, e.g., about 10–15 MHz ($(3–5) \times 10^{-4}$ cm^{-1}, 4–6 G). (2) It is not possible to match the experimental spectrum using simulations based upon one particular orientation of the g-tensor. This is consistent with the imidazole rings adopting a range of rotational orientations in solution.[68] It is interesting to note that the previously reported EPR spectra of low-spin iron porphyrins in glassy solutions do not resolve the differences in the direction of the x,y axes. However, their g-values are similar to

(65) (a) Eaton, G. R.; Eaton, S. S. *Acc. Chem. Res.* **1988**, *21*, 107–113 and references therein. (b) Eaton, S. S.; More, K. M.; Sawant, B. M.; Boymel, P. M.; Eaton, G. R. *J. Magn. Reson.* **1983**, *52*, 435–449.

(66) *Topics in Current Physics*; Binder, K., Ed.; Springer-Verlag: New York, 1986; Vol. 7.

(67) Raitsimring, A. M.; Basu, P.; Enemark, J. H. Manuscript in preparation.

(68) Walker, F. A.; Huynh, B. H.; Scheidt, W. R.; Osvath, S. R. *J. Am. Chem. Soc.* **1986**, *108*, 5288–5297.

those of the crystalline form,[68] which was later shown[69] to have the imidazole planes lying close to the N–Fe–N porphyrin axes, suggesting that this is the lowest energy form.[68] The Mo(V) center of **13** is sensitive to the geometrical details of the imidazole interaction and thereby allows an independent assessment of the relative preference for axial ligand orientation (and hence in-plane anisotropy). It is entirely possible that the steric requirements of **13** and **14** result in the preferred orientation of the axial ligand planes being close to bisecting the N–Fe–N axes rather than approximately eclipsing them, as in the earlier study.[68,69]

Before discussing the results of the detailed simulations of **14** with various values of the exchange interaction, it should be noted that the exchange interaction itself does not change the line widths of the two paramagnetic centers. However, if one of the centers has a short relaxation time, then the exchange interaction will cause the relaxation time of the second center to become the same as the first and thereby induce line broadening of the second center. The Mo(V) part of the EPR spectrum of **14** exhibits a rather broad line width which is likely induced by the fast relaxation of Fe(III). To prove this possibility, the EPR spectrum of **14** was also measured at 4.2 K in order to increase the relaxation time of iron(III). However, the spectrum at 4.2 K was identical to that at 77 K. Therefore, the initial line width of Mo(V) and a distribution of J-values were used to simulate the spectrum of **14**. Reasonable agreement between experimental and simulated spectra was achieved when a rectangular distribution of J-values in the range of 100–2000 MHz ((3.34–66.7) × 10^{-3} cm^{-1}) was used. Figure 10 shows the integrated spectrum that results from this simulation using a step size of 100 MHz (3.34 × 10^{-3} cm^{-1}). This relatively coarse step size creates artifacts in the derivative spectrum, but the simulated absorption spectra is in reasonable agreement with experiment. Since the dipole–dipole interaction is not dominant for **14**, information about the geometrical relationship between the two metal centers is lost. A range of exchange interactions is consistent with a range of rotational orientations of the axial imidazole ligands (*vide supra*).

Summary

Tetraarylporphyrins possessing a single pendant catechol group at one of the meso carbon atoms provide a relatively rigid organic framework for initial quantitative modeling of the inter-prosthetic group interaction between the molybdenum and iron centers of sulfite oxidase. This study has concentrated on these interactions in stable complexes that possess oxo-Mo(V) and low-spin Fe(III) porphyrin centers with Mo···Fe distances of 7.9 and 9.4 Å. The spectroscopic and electrochemical data clearly show that the individual centers retain their identities and are only slightly perturbed by the weak coupling between the two paramagnetic metal centers.

Quantitative investigation of the coupling between the oxo-Mo(V) and low-spin Fe(III) porphyrin centers by EPR spectroscopy shows that the primary mechanism for coupling changes with distance. For **14**, the Mo···Fe distance is about 7.9 Å, and the primary interaction is weak exchange coupling of (3–60) × 10^{-3} cm^{-1} ((0.1–2) × 10^3 MHz). For **13**, with an Mo···Fe distance of 9.4 Å, the exchange contribution through the pendant aromatic catechol ring is negligible, and weak anisotropic dipolar coupling is the primary interaction between the two $S = {}^1/_2$ spin centers. The dependence of dipolar coupling upon the Mo(V)···Fe(III) distance means that the compounds related to **13** that possess longer Mo···Fe distances will be fruitful synthetic models for further quantitating the dependence of the anisotropic dipolar coupling between oxo-Mo(V) and low-spin iron porphyrin centers upon distance and molecular geometry.

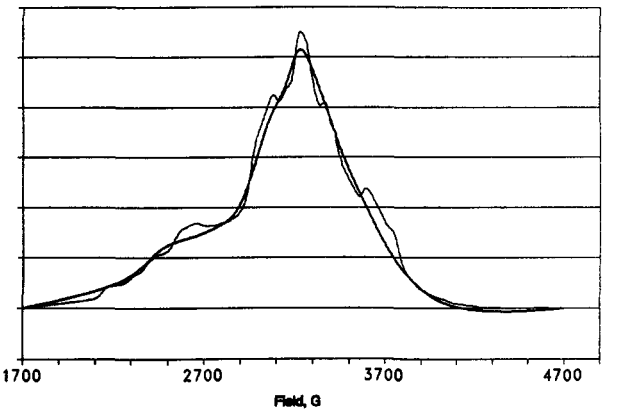

Figure 10. Integration of the experimental (bold line) and simulated (light line) EPR spectra of **14** in 1:1 dichloromethane–toluene glass. The small, uncoupled Mo(V) impurity signal (Figure 8) has been subtracted from the observed spectrum.

For sulfite oxidase, the Mo···Fe distance is likely to be at least 9.4 Å. To our knowledge, dipolar coupling between the metal centers has not yet been observed in the enzyme. However, the EPR results for **13** strongly suggest that a careful EPR study of the Mo(V)···Fe(III) state of the sulfite oxidase may provide insight concerning the inter-prosthetic group distance in the enzyme.

Finally, we are aware that the present models do not incorporate sulfur ligation of the molybdenum atom as occurs in sulfite oxidase. For **13** and **14**, the Fe(III) center is more easily reduced than Mo(V). Incorporation of sulfur coordination to the molybdenum atom and modulation of the aryl groups of the porphyrin should lead to bimetallic systems in which the Mo(V) center is more easily reduced[16,59] and to systems where the Mo(V/IV) and Fe(III/II) reduction potentials of the two metal centers are nearly identical to one another. Ongoing research is directed to synthesizing such model systems, investigating electron-transfer reactions in these systems, and probing the subtle magnetic coupling interactions between the paramagnetic centers of other metalloporphyrins possessing pendant oxo-molybdenum(V) units.[70]

Acknowledgment. We acknowledge Professor F. A. Walker for numerous helpful and stimulating discussions. We thank Dr. M. A. Bruck for his help with computer applications. Support of this research by the National Institutes of Health (GM-37773 and NIH2SO3RR03495-04) and the Materials Characterization Program of the University of Arizona is gratefully acknowledged. We thank the National Science Foundation (DIR-9016385) for funds for the purchase of the EPR spectrometer.

Supplementary Material Available: Proton NMR spectra of **13** and **14** (2 pages). This material is contained in many libraries on microfiche, immediately follows this article in the microfilm version of the journal, and can be ordered from the ACS; see any current masthead page for ordering information.

(69) Soltis, S. M.; Strouse, C. E. *J. Am. Chem. Soc.* **1988**, *110*, 2824–2829.

(70) Basu, P.; Raitsimring, A.; Enemark, J. H. Unpublished results.